Optimal Operation of Distributed Energy Storage Systems to Improve Distribution Network Load and Generation Hosting Capability

Nadeeshani Jayasekara, *Student Member, IEEE*, Mohammad A. S. Masoum, *Senior Member, IEEE*, and Peter J. Wolfs, *Senior Member, IEEE*

***Abstract*—This paper proposes a strategy for optimal integration of battery energy storage systems (BESSs) to improve the load and distributed generation (DG) hosting ability of the utility grid. An effective tool that determines the optimal capacity and day-ahead operation strategy for deployment of distribution network operator (DNO)-controlled BESSs is presented. It is a cost-based multiobjective optimization strategy that considers two primary factors: 1) distribution system cost; and 2) battery cycling cost. Quantitative analyses on the benefits and tradeoffs of BESS installations are carried out considering different service options. BESS is investigated for three main service options: 1) voltage regulation; 2) loss reduction; and 3) peak reduction. The performance and benefits of the optimized BESS to control one service option exclusively or multiple services simultaneously is compared. The analysis is further extended to study the effect of installation site on the size, management strategy, and the service option. Results show that optimal integration of BESSs can realize maximum operational and cost benefits while effectively elevating the load and DG hosting capability of the network. The approach is developed using MATLAB interior-point algorithm. Simulations are conducted for the medium voltage (MV) IEEE 33 bus system and a low voltage (LV) distribution network in Western Australia studied during the Perth Solar City Trial.**

***Index Terms*—Battery storage, charge/discharge management, dispatch management, optimal siting, optimal sizing, predictive optimization.**

I. Introduction

THE integration of large quantities of renewable generation is critical to ensure energy availability while minimizing the carbon footprint [1], [2]. In order to address these concerns, several policies and subsidies have been established globally to support the deployment of nonhydro renewable distributed generation (DG), particularly wind and photovoltaic (PV). These measures along with the recent technology advancements have attracted investments in both private and government sectors to help with transforming the typically monopolistic market [3]. As a result, a rapid expansion of PV generation has occurred in the recent years. These trends in the adoption of PV and technology developments propose that traditional centralized paradigm might change in the years to come, converting the existing grid to a decentralized power system with bidirectional power flow [2]. The successful implementation of a dynamic decentralized network will require advanced metering infrastructures (AMIs) and the convergence of information and communication technology (ICT) with power engineering [4]. This conceptual design is referred to as "smart grid" [5], [6]. Successful implementations of smart grids are expected to be highly energy-efficient and reliable with high levels of PV [7].

However, the development of decentralized grid is impeded by concerns over uncertainties associated with variability, location, and coordination of available renewable capacities [8]. The variability of PV output mainly affects the operation of generation sources in the mix, whereas its location and modularity will impact the performance of the grid especially in terms of voltage profiles [9].

Battery energy storage system (BESS) is increasingly becoming popular as a solution that facilitates seamless integration of DGs [10], [11]. Capacity support, congestion management, transmission and distribution loss reduction, voltage regulation, deferral of upgrade investments, reduction of peak demand charges, and improved power quality are some benefits of combining BESSs with high penetrations of PV [10], [12]. At present, cost of batteries is the main barrier preventing their adoption. Therefore, optimal integration and a better understanding of capabilities and the role of BESS in the capacity mix are needed to realize maximum techno-economic benefits for the grid while improving the battery cost competitiveness.

In [13], a method is proposed for home area energy management using energy storage to facilitate demand response management. An optimal predictive power scheduling battery management algorithm for peak load shaving is presented in [14]. Two rule-based control techniques for storage dispatch control are proposed in [15] and [16]. The primary objective of papers [15] and [16] is peak shaving. The rule-based or real-time strategies do not consider daily cycling of the battery. Therefore, the proposed strategies cannot optimize the battery techno-economic performance. In addition, papers [15] and [16] do not discuss the problem of optimal placement and sizing. This is a crucial problem, as the benefits of BESS strictly depend on the location and sizing [17]. Methods for optimal placement and sizing of storage are proposed in [18] and [19],

Manuscript received July 03, 2014; revised November 11, 2014, February 11, 2015, and July 22, 2015; accepted September 03, 2015. Paper no. TSTE-00336-2014.

N. Jayasekara and M. A. S. Masoum are with the Department of Electrical and Computer Engineering, Curtin University, Perth 6000, W.A., Australia (e-mail: m.jayasekara@student.curtin.edu.au; m.masoum@curtin.edu.au).

P. J. Wolfs is with the Power and Energy Centre, Central Queensland University, Rockhampton 4700, Qld., Australia (e-mail: p.wolfs@cqu.edu.au).

Color versions of one or more of the figures in this paper are available online at http://ieeexplore.ieee.org.

Digital Object Identifier 10.1109/TSTE.2015.2487360

respectively. However, they do not deal with the problem of optimal management.

This paper proposes a strategy for optimal integration of distribution network operator (DNO)-owned BESSs to improve the load and DG hosting ability of the grid. This paper addresses the issues of optimal management and sizing of a community-scale BESS for distribution systems with high penetrations of DG. A cost function that incorporates costs incurred due to peak support, distribution system losses, poor voltage levels, and battery cycling is developed for the derivation of the optimal battery management strategy. BESS management strategy optimizes the day-ahead operation of the battery storage by controlling the battery external parameters including charge/discharge rates, depth of discharge (DOD), and daily cycling. Day-ahead scheduling determines the extent to which source (grid or BESS) operates at any given time interval, amount of power exchange, direction of power flow, and the mode of operation at the point of common coupling. Optimized battery operation patterns are then utilized to evaluate the optimal BESS capacity requirements. Optimal installation sites are chosen as the buses at which the cost function is at minimum. This paper also provides a review on usage of storage for the exclusive and simultaneous control of voltage regulation, peak demand, and loss reduction. A quantitative analysis on the impact of installation site on the purpose of installation, dispatch management scheme, and size of BESS is also carried out.

II. Battery Energy Storage

A. Battery Energy Storage Systems

Deployment of BESS has been uneconomic due to high capital operation and maintenance (O&M) expenses. However, the cost of battery storage is steadily reducing with the recent advances in battery technologies and competitive manufacturing in the vehicle market [20]. Reference [21] suggests that with current falling PV prices, "grid parity" against retail electricity prices could be achieved if battery storage prices drop to 20 cents per kWh.

Fig. 1(a) demonstrates the capacity and impedance as a function of cycling for a 12V A123 ALM 12V7 Lithium-ion (Li-ion) battery rated at 4.6 Ah/10 A [22]. From Fig. 1(a), at the 1C/1C rate and 100% DOD, the battery delivers more than 7000 cycles with an excellent energy preservation capability. Fig. 1(a) shows that the internal cell impedance is a function of cycle life. The terminal voltage characteristics against the discharging capacity at various discharge rates are illustrated in Fig. 1(b). Battery voltage is almost flat in the region between 0% and 90% discharge capacity and rapidly drops over 90% discharge capacity. Thus, it is advisable to operate Li-ion batteries within this region.

The state of charge (SoC) and state of health (SoH) are two key measures that represent the battery-operating condition and performance [23]. SoC indicates the amount of available energy relative to the real maximum capacity of the battery (1). Capacity deviation due to battery cycle ageing and temperature

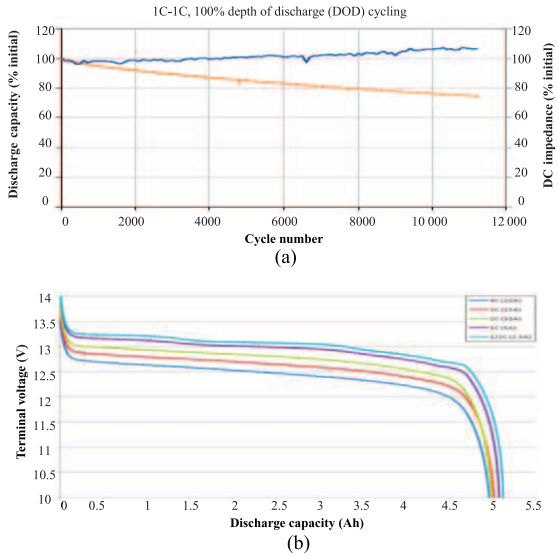

Fig. 1. (a) Capacity and impedance as a function of cycling at room temperature. (b) Terminal voltage against discharge capacity at various discharging rates and 40 °C [22].

effects is presented using SoH. SoH is the ability to store energy relative to its nominal capability (2) [24]

$$\mathrm{SoC}(t) = \mathrm{SoC}\,(0) + E_B(t)/E_{B-\mathrm{act}}(t) \quad (1)$$

$$\mathrm{SoH}(t) = E_{B-\mathrm{act}}(t)/E_{B-\mathrm{nom}} \quad (2)$$

where t, $\mathrm{SoC}\,(0)$, E_B, $E_{B-\mathrm{act}}$, and $E_{B-\mathrm{nom}}$ are the time, initial SoC, battery capacity, actual battery capacity, and nominal capacity, respectively.

The $E_{B-\mathrm{act}}$ (1)–(2) encompasses a linear and a nonlinear term. Linear component (E_B) can be derived using the daily cyclic behavior. Nonlinear component reflects the effect of daily cycling and operating temperature on the battery internal parameters [23], [24]. Hence, typically the nonlinear component cannot be measured directly and may require mathematical estimation models like that derived in papers [23]–[25]. Both linear and nonlinear elements strongly depend on the daily cycling. Thus, given that battery is operated within the nominal temperature range, the cycling primarily contributes to the capacity degradation [25]. Therefore, with increased charge/discharge cycles, cycle age of the battery decreases.

The proposed battery control strategy for feeder quality management effectively minimizes daily cycling through optimal charge/discharge and DOD management. Therefore, the life expectancy of BESS is extended by avoiding wear and tear due to unnecessary cycling. Extended cycle life translates to lower ownership costs improving the performance and value.

B. Modeling of BESS

The BESS dispatch optimization problems rely on the repeated evaluation of a solution vector of battery power or energy. The length of the vector depends on the sampling interval. The solution could be a sequential list of the energy values

($\boldsymbol{C}_{iT}$) during the day as shown in (3). A vector of length (m) 24, 48, or 96 could list the E_B at 1-h, 30-min, or 15-min intervals.

$$\boldsymbol{C}_{iT} = \begin{bmatrix} E_B\,(1) \\ \vdots \\ E_B\,(m) \end{bmatrix} \tag{3}$$

This vector should be subject to the following.

1) A daily energy balance constraint. This avoids over charging or discharging at the end of a cycle and correctly sets the battery for flexible operation on the following day.
2) Charging and discharging power constraints. Only limited differences can exist between any two adjacent charge states.
3) A solution vector presented as a list of power is resistant to efforts to compactly represent the solution. Power can be a discontinuous function and the daily charging power frequency spectrum has increased higher frequency components relative to the energy spectrum.

Each constraint vector could be of the same dimension; thus, add extra burden on the optimization. A superior approach (implemented in [26]) is to represent the periodic battery energy solution utilizing a vector of Fourier coefficients ($\boldsymbol{C}_{iF}$) such that:

$$\boldsymbol{C}_{iF} = \begin{bmatrix} a_1, b_1 \\ \vdots \\ a_m, b_m \end{bmatrix} \tag{4}$$

$$E_B(t) = a_0 + a_1 \cos\left(\frac{2\pi t}{T}\right) + b_1 \sin\left(\frac{2\pi t}{T}\right) + \cdots + a_m \cos\left(\frac{2\pi m t}{T}\right) + b_m \sin\left(\frac{2\pi m t}{T}\right) \tag{5}$$

where a_0, a_m, b_m, m, and T are the constant Fourier coefficient, Fourier cosine coefficients, Fourier sine coefficients, number of Fourier coefficients (set to 8 [26]), and period, respectively.

The vector $\boldsymbol{C}_{iF}$ represents the battery energy which is, by definition of (5), periodic and continuous, thus inherently encapsulates the above constraints. The compact representation, therefore, reduces the dimensionality of the optimization problem and improves the computational efficiency while effectively maintaining the periodicity and continuity of the battery energy function.

The coefficient a_0 does not need to be included in the solution vector $\boldsymbol{C}_{iF}$. The presence of a constant does not affect the battery charge or discharge power and has no impact on the daily energy cost. The coefficient a_0 can be set after the optimization process to ensure that battery energy curve is not negative or lower than an operationally required minimum charge value based on the DOD requirements.

Battery power can be found as the difference between two consecutive charge states as shown in (7) and (8). The generator convention is applied, and the charging power of the battery is considered positive and discharging power to be negative.

$$\Delta E_B = E_B(t) - E_B\,(t-1) \tag{6}$$

$$P_B(t) = \Delta E_B / \left(\Delta t \times \eta_c\right), \quad \text{if } P_B(t) > 0 \tag{7}$$

$$P_B(t) = \Delta E_B \times \eta_d / \Delta t, \quad \text{if } P_B\,(\mathrm{t}) < 0 \tag{8}$$

where $\eta_c = \eta_d = \sqrt{\eta_{\text{bat}}}$, $\eta_{\text{bat}} = 0.9$ is the battery round trip cycling efficiency, η_c, η_d, P_B, and Δt are battery charging efficiency, discharging efficiency, battery power, and sampling interval, respectively.

Inclusion of the battery cycling efficiency in the battery model promotes further reductions in the daily SoC swing, optimizing the cycle life. Size of the BESS (9) is found as the difference between the maximum and the minimum battery energy (found from optimization for different seasons) divided by the maximum DOD (DOD_{max}).

$$\text{Battery size (kWh)} = \frac{\left|{E_B}^{\max} - {E_B}^{\min}\right|}{\text{DOD}_{\max}} \tag{9}$$

where $\text{DOD}_{\max} = 0.8$. ${E_B}^{\max}$ and ${E_B}^{\min}$ are the maximum and minimum battery energy, respectively.

The battery daily cycles and life in years can be evaluated from (10) and (11), respectively,

$$\text{Cycles} = \frac{1}{2}\frac{\sum_{t=1}^{T} |E_B(t) - E_B\,(t-1)|}{\text{DOD.BatterySize}} \tag{10}$$

$$q\,(\text{years}) = \text{CycleLife}/\left(\text{Cycles}.D\right) \tag{11}$$

where Cycle, $D = 285$ days, CycleLife = 3000 cycles, and q are the number of daily battery cycles, number of operating days, nominal cycle life of BESS, and the battery's real life in years, respectively.

Power balance at interconnection point can be defined as:

$$P_i(t) = P_{\text{inv}-i}(t) - P_{L-i}(t) \tag{12}$$

$$P_{\text{inv}-i}(t) = \begin{cases} [P_{\text{DG}-i}(t) - P_{B-i}(t)].\eta_{\text{inv}}, & \text{if } P_{\text{inv}-i}(t) > 0 \\ [P_{\text{DG}-i}(t) - P_{B-i}(t)]\,/\eta_{\text{inv}}, & \text{if } P_{\text{inv}-i}(t) < 0 \end{cases} \tag{13}$$

where i is the bus number $i = 1, 2, \ldots, n$, P_i, P_{L-i}, $P_{\text{inv}-i}$, $P_{\text{DG}-i}$, and η_{inv} are bus power, active load power, inverter power, generation from inverter interfaced DG, and inverter efficiency, respectively.

III. Problem Formulation

A. Objective Function

The cost function in (14) is constructed to minimize distribution system costs (C_{system}) in terms of costs incurred due to system losses (C_{Loss}), peak demand (C_P), and voltage regulation (C_{VR}). Planning problem should contain the investment and operating costs of battery to optimize benefit tradeoffs. Hence, a cost factor that represents BESS capital and O&M expenditures (C_{battery}) in a form of a daily cost is included in the objective function:

$$f\left(\boldsymbol{C}_{iF}\right) = \sum_{l=1}^{4} \gamma_l.f_l = \gamma_1 C_{\text{battery}} + \gamma_2 C_{\text{Loss}} + \gamma_3 C_{\text{VR}} + \gamma_4 C_P \tag{14}$$

where $C_{\text{system}} = \gamma_2 C_{\text{Loss}} + \gamma_3 C_{\text{VR}} + \gamma_4 C_P$

$$C_{\text{Loss}} = \int_{t=1}^{T} \sum_{k=1}^{n-1} |\left\{ {V_j}^2(t) + {V_i}^2(t) - 2V_i(t)V_j(t) \times \cos\left(\delta_i(t) - \delta_j(t)\right)\right\}| . G_{ij} . \Delta t . r_{\text{loss}}(t) . dt$$

$$C_{\text{VR}} = \int_{t=1}^{T} \sum_{i=1}^{n} |{|V_i(t)|}^2 - {V_{\text{ref}}}^2|^{1/2} . \Delta t . r_{\text{VR}}(t) dt$$

$$C_P = P_{\max} . \Delta t . r_p$$

$$C_{\text{battery}} = \frac{\text{Cycles}}{\text{CycleLife}} . \text{BUC} . \text{BatterySize} .$$

$$\gamma_l = w_l / J_l .$$

In the above equations, V_i, δ_i, G_{ij}, $V_{\text{ref}} = 1$ p.u., $P_{\max}$, $r_{\text{loss}} = 28.4\text{c/kWh}$, r_{VR}, r_p, battery unit cost (BUC) $= 300\$/\text{kWh}$, γ_l, w_l, and J_l are the voltage magnitude, voltage angle, conductance of branch k, reference voltage at slack bus, maximum power seen at distribution transformer over the period, loss cost rate, voltage regulation cost rate, peak demand cost rate, battery unit cost, scaling factor, weighting factor ($\sum_{l=1}^{4} w_l = 1$, equally weighted), and J_l is the minimum of f_l [27], respectively.

The following points are highlighted on the proposed BESS management strategy.

1) The primary inputs to the optimization problem are network characteristics, time-variant load and generation forecasts at 15-min interval, and an initial vector of the control variable, Fourier coefficient vector ($\boldsymbol{C}_{iF}$). The secondary inputs include battery and network constraints and the cost coefficients (r_{loss}, r_{VR}, r_p, and BUC).
2) The direct output is the optimized Fourier coefficient vector, while BESS charge/discharge schedule (7), (8), BESS energy profile (5), power flow coordination (12), and optimal BESS size (9) can be derived using the optimized $\boldsymbol{C}_{iF}$. The optimization problem is a nonlinear constrained problem that is solved using MATLAB interior-point algorithm.
3) The r_{loss} is the electricity price taken from [28] for Western Australia. This cost comprises four main components: 1) retail; 2) wholesale energy; 3) transmission; and 4) distribution costs. Out of this, wholesale energy and distribution costs are the major drivers representing more than 70% of the aggregated electricity price. The electricity price also reflects the costs of upgrades, O&M, and reinforcements driven by voltage and thermal limit violations as well as recovery costs of incentive schemes and carbon costs [28].
4) The factor r_p is the peak demand charge assumed at $\$200/\text{kWh/year}$. This is typically made up of peak support, demand supply capital, maintenance, and infrastructure development costs [29].
5) Rate of voltage violations due to peak generation and load is represented by $r_{\text{VR}} = 14.2\text{c/kWh}$. This rate reflects the network charges and is about 50% of the end user electricity price [29]. The C_{VR} encourages voltages to the nominal V_{ref}. Most utility providers prefer near unity voltages. In the IEC61000, the voltage limits are now supplemented by "preferred ranges."
6) Cost function will not consider the transmission costs for two main reasons: 1) the transmission cost component is generally a small fraction of the aggregated electricity price seen by consumers; and 2) existing transmission lines have been developed with the aim of transporting electricity produced by centralized large scale generators. Improving the DG hosting ability of the low voltage (LV) grid through optimal integration of BESS reduces the power that needs to come from centralized sources. Hence, minimization of LV distribution cost will coincidentally reduce transmission and carbon emission costs.
7) In regards to the battery cost, the C_{battery} component assesses the battery cyclic performance and eliminates unnecessary cycling to minimize wear and tear. BUC is a representative daily cost that combine capital O&M costs of battery. In this paper, SoC is expressed in terms of the original capacity and it is assumed that battery operates within the name plate ranges for temperature and charge/discharge rates. This is sufficient, as the batteries in this application operate with relatively few daily cycles and at moderate rates. Deep discharges or overcharging is easily avoided by setting appropriate operational limits. Hence the C_{battery} economically captures charging and discharging cycles improving the battery efficiency and cycle life while reducing the linear daily SoC swing and DOD.

Note that the optimal parameters and benefits of BESS depend on the services to be provided. Therefore, this paper derives optimal BESS parameters considering the minimization of complete cost function defined in (14) and individual cost factors that constitute C_{system}, for benefits and tradeoffs quantification.

B. Objective Function Constraints

1) Voltage Constraint: The optimization is required to comply with the inequality voltage constraint in (15).

$$V_{\min} < \left|{V_i}^t\right| < V_{\max} \tag{15}$$

where $V_{\min}$ and $V_{\max}$ are the lower and upper voltage limits, respectively. The West Australian Technical Rules and Electricity Act 1945 section 25(1)(d) require the steady-state voltage to be within $\pm 6\%$ of the nominal voltage during normal conditions.

2) VUF Constraint: For three-phase unbalanced systems, a voltage unbalance factor (VUF) can be defined as:

$$\text{VUF} = \sum_{i=1}^{n} \frac{{V_i}^2}{{V_i}^1} .100 \tag{16}$$

where V^2 and V^1 are the positive and negative sequence voltages, respectively.

The VUF constraint is expressed as:

$$\text{VUF} < \text{VUF}_{\max} \tag{17}$$

where $\text{VUF}_{\max} = 1$ is the maximum VUF.

3) Battery Constraints: Below battery constraints are established for added security to ensure that battery power or energy does not exceed their boundary limits during charge/discharge management:

$$P_{B-\min} < P_B < P_{B-\max} \tag{18}$$

$$E_{B-\min} < E_B < E_{B-\max} \tag{19}$$

where $P_{B-\min}$, $P_{B-\max}$, $E_{B-\min}$, and $E_{B-\max}$ are lower and upper limits of P_B, and lower and upper limits of E_B, respectively.

The above constraints can be added to the cost function as a penalty cost rather than separate constraints if required. The battery constraints were not imposed in the optimization to facilitate the problem of sizing in this paper.

C. Providing the Jacobian of Cost Function and Constraints

The nonlinear optimization problem (14) is solved using the interior point (IP) method. The standard IP method is computationally very expensive and the computational burden increases with the size of the problem and network topology. This is because it uses finite-difference method to determine the gradients of the cost function and constraints to evaluate Lagrangian and first-order optimality equations. Instead, in this paper, analytical gradient (Jacobian) of the cost function and constraints are provided to improve the optimization efficiency [30]. Jacobians are found with respect to Fourier coefficients as shown in (20) and (21); $\frac{dV_i}{dP_i}$ is found from the inverse power flow Jacobian. Analytical gradient also improves the numerical conditioning of the iterative process.

$$\nabla f = \left[\frac{dC_{\text{system}} + C_{\text{battery}}}{dx_p}\right] = \left[\frac{dC_{\text{system}}}{dx_p} + \gamma_1 \frac{C_{\text{battery}}}{dx_p}\right] \tag{20}$$

where p is the Fourier coefficient number $p = 1, 2, \ldots, (mx2)$ and,

$$\frac{dC_{\text{system}}}{dx_p} = \left[\gamma_2 \frac{dC_{\text{Loss}}}{dV_i} \cdot \frac{dV_i}{dP_i} + \gamma_3 \frac{dC_{\text{VR}}}{dV_i} \cdot \frac{dV_i}{dP_i}\right] \cdot \frac{dP_i}{dx_p} + \gamma_4 \frac{dC_P}{dP_i} \cdot \frac{dP_{\max}}{dx_p}.$$

Jacobian of the inequality constraints are derived as:

$$J_g = \begin{bmatrix} -\frac{dV_i}{dP_i} \cdot \frac{dP_i}{dx_p} & \frac{dV_i}{dP_i} \cdot \frac{dP_i}{dx_p} \\ -\frac{dP_B}{dx_p} & \frac{dP_B}{dx_p} \\ -\frac{dE_B}{dx_p} & \frac{dE_B}{dx_p} \end{bmatrix}^T \tag{21}$$

It was found that providing the Jacobian or gradient for cost and constraints improves the optimization speed by over 80% (average from 15 runs).

D. Summary of the Proposed Management Architecture

This paper proposes a receding horizon hierarchical control approach for BESS management. The structure of the system is presented in Fig. 2. Central controller performs the proposed

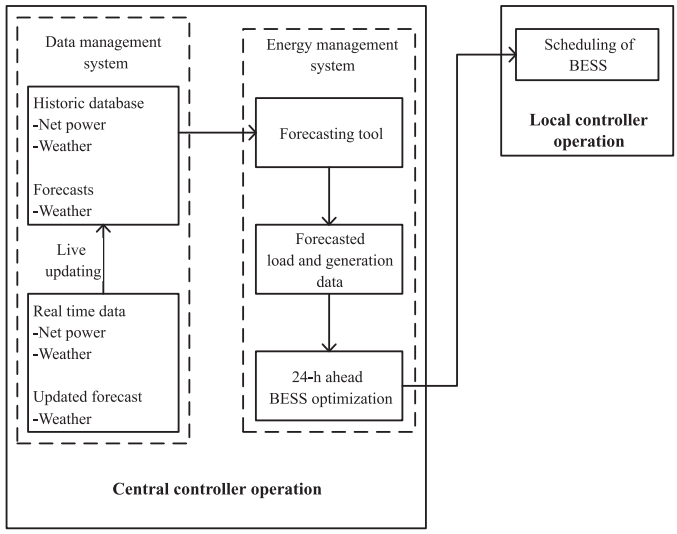

Fig. 2. Proposed system architecture.

predictive optimization to identify the optimal parameters of BESS. It is composed of two systems: 1) data management system (DMS); and 2) an energy management system (EMS). DMS establishes a bidirectional communication link with the network for online data acquisition. By centralizing the information and controls, the DMS is able to consistently monitor the performance and provide safety oversights.

Collected data are then fed to EMS. The EMS first carries out the forecasting of the load and generation data 24 h into the future. The BESS management system (BMS) uses the forecasted load data to solve the optimal power flow management problem. BMS returns the optimized $\boldsymbol{C}_{iF}$. Optimal Fourier coefficient vector determine the dispatch schedule of the BESS in terms of charging/discharging response and energy. The EMS then sends the optimized battery set-points for day-ahead scheduling of the BESS to the local controller in the power electronic interface.

The control algorithm can be reapplied several times each day to allow the battery energy profile to be progressively updated, as new information and trends emerge in the operating distribution network. The new predicted battery charge profile $E_{B-\text{new}}(\phi)$ is then used to update the previously optimized energy profile $E_{B-\text{old}}(\phi)$ for the current updating time step (ϕ). Updating could be performed using an exponential smoothing technique:

$$E_{B-\text{updated}}(\phi) = \alpha . E_{B-\text{new}}(\phi) + (1-\alpha) E_{B-\text{old}}(\phi) \tag{22}$$

where α is the smoothing factor and $0 < \alpha < 1$.

E. Summary of the Proposed BESS Management and Sizing Approach

The following procedure is adopted for optimal management and sizing of BESS.

Step 1) Determine the candidate buses based on geographical and other planning constraints.

Step 2) Adjust the cost function depending on the optimization objective features required.

a) For multiobjective placement and sizing (14)

$$f = C_{\text{system}} + \gamma_1 C_{\text{battery}}.$$

b) For pure control of distribution system cost factors, the optimization cost function can be adjusted as follows.

i) For voltage regulation

$$f_{\text{VR}} = \gamma_3 C_{\text{VR}} + \gamma_1 C_{\text{battery}} \tag{23}$$

ii) For loss reduction

$$f_{\text{loss}} = \gamma_2 C_{\text{Loss}} + \gamma_1 C_{\text{battery}} \tag{24}$$

iii) For peak shaving

$$f_P = \gamma_4 C_P + \gamma_1 C_{\text{battery}} \tag{25}$$

Step 3) Run the optimization with BESS at each selected bus, one at a time. The optimization will return:

a) value of cost function;

b) corresponding Fourier coefficient vector.

Step 4) Locate the optimal bus at which cost function is minimal.

Step 5) Obtain the optimized battery energy profile using the optimized Fourier coefficient vector found for optimal bus in Step 4).

Step 6) Battery size can be evaluated from (9).

The approach for sizing and siting should be tested using data for all seasons to capture seasonal variations in the generation and load patterns. Site is determined as the location that offers maximum tradeoffs and size of the BESS can be determined as the maximum found from optimization for different seasons.

IV. Test Systems

The proposed approach is tested on a medium voltage (MV) and an LV distribution system. The voltage dependency of the loads is modeled using polynomial equations:

$$P_{L-i} = P_{0i}\left(a_p + b_p\left|V_i\right| + c_p\left|V_i\right|^2\right) \tag{26}$$

$$Q_{L-i} = Q_{0i}\left(a_q + b_q\left|V_i\right| + c_q\left|V_i\right|^2\right) \tag{27}$$

where $Q_{L-\text{i}}$ is the reactive power load, $a_p + b_p + c_p = 1$, and $a_q + b_q + c_q = 1$.

In this paper, load flow calculations are performed using the total current injection method (TCIM) in [31] and [32] and bus 1 is considered as the slack bus with a voltage of 1 p.u.

A. MV Test System—Case 1

In Case 1, the proposed approach is tested on the hypothetical IEEE 33-bus distribution system of Fig. 3. Complete system data can be found in [33]. The substation voltage of the test system is 12.66 kV and the base is chosen as 10 MVA.

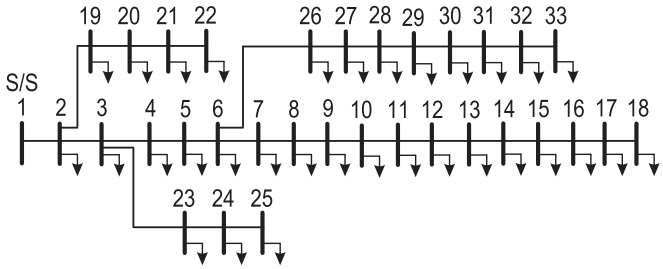

Fig. 3. Single-line diagram of IEEE 33 bus distribution system.

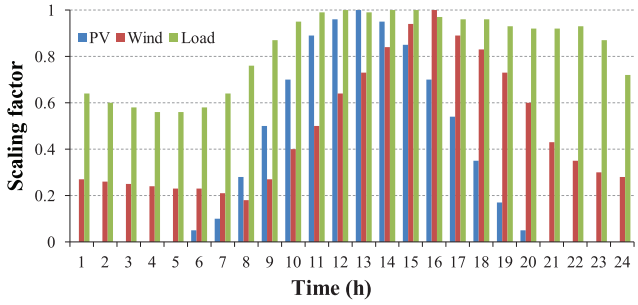

Fig. 4. Scaling factors of time-variant load and generation.

Two wind-based DGs and seven PV DGs were allocated to simulate a high DG penetration scenario. PV DGs could represent aggregated generation seen at the installed bus. Two wind DGs of 1 MW are sited at buses 18 and 24. Three 400-kVA PV DGs are installed at buses 5, 21, and 31 and four 500-kVA PV DGs are installed at buses 8, 12, 28, and 33.

It was assumed that the loads follow the IEEE-RTS model as illustrated in Fig. 4 [34] and the load composition was set to $a_p = a_q = 0.4$, $b_p = b_q = 0.3$, and $c_p = c_q = 0.3$. Peak active and reactive load power of the system with the above load composition are 3.556 MW and 2.191 MVar, respectively. The output generation from wind and PV DGs are expected to follow the curves in Fig. 4 [35].

B. LV Test System—Case 2

In Case 2, the proposed approach is tested on an LV distribution system studied under the Perth Solar City Trial. System is depicted in Fig. 5. Each load is modeled with a colocated rooftop PV system. Network is supplied by a 200-kVA 22 kV/415 V distribution transformer. The consumer mains are of 6 mm^2 copper with R = 3.7 Ω/km and X = 0.369 Ω/km while the aerial mains are of two all-aluminum conductors (AACs) of types: 7/4.50AAC and 7/3.75AAC. The simulations are conducted assuming balanced conditions.

V. Results and Discussion

The optimization determines the battery optimal charge/discharge strategy and the size which in turn coordinates the power flows at the interconnection point. Simulations were conducted for the optimization of 1) voltage regulation [f_{VR} defined in (23)]; 2) loss reduction [f_{loss} defined in (24)]; 3) peak reduction [f_p defined in (25)]; and 4) multiple services

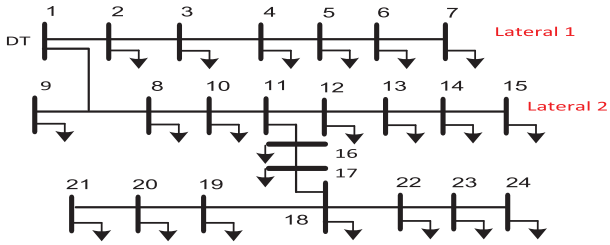

Fig. 5. LV test model.

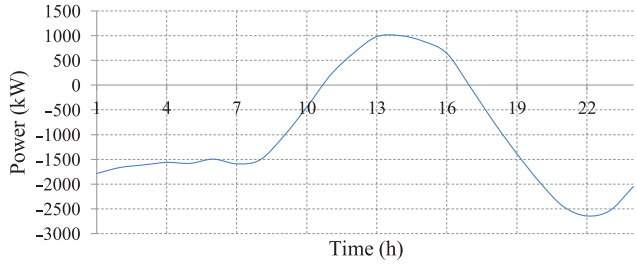

Fig. 6. Distribution transformer loading with no BESS.

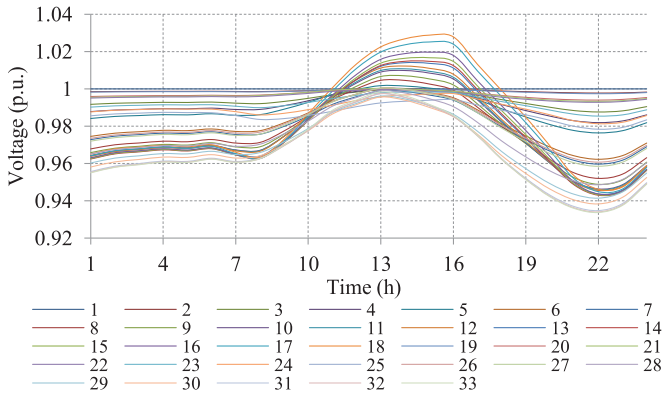

Fig. 7. Voltage profile with no BESS at each bus.

simultaneously [f defined in (14)]. The installation site is determined as the bus at which the cost function is minimal. A quantitative analysis on the effect of installation site on the optimal battery parameters and grid services to be provided is carried out in this section.

A. Test Case 1—MV Distribution System

1) Base Operation With No BESS: Figs. 6 and 7 graphically illustrate the net distribution transformer load (without losses) and the voltage profile, respectively, without BESS. The system clearly experiences reverse power flow and overvoltage issues that are recognized as the major limiting factors for the widespread uptake of renewable DG. The peak export power is 1.002 MW and the maximum voltage is 1.028 p.u. at bus 18. The total load energy demand is 71.2005 MWh.

2) Simulation Results: Table I summarizes the simulation results of the optimal size, site, BESS life expectancy, voltages (minimum and maximum), peak power, and losses for different service options. The buses 26, 24, 12, and 27 are identified as the installation sites when optimizing for f_{VR}, f_p, f_{loss}, and f, respectively. Figs. 8–10 show the resultant battery

TABLE I
SUMMARY OF RESULTS FOR TEST CASE 1

Cost func.	Site (bus no.)	Voltage (p.u.)		E_{loss} MWh	P_{max} MW	Battery	
		Min (bus#)	Max (bus#)			Size (MWh)	Life (years)
Base		0.934 (33)	1.028 (18)	1.79	2.642		
f_{VR}	26	0.960 (30,32, 33)	1.006 (18)	1.57	1.323	14.42	10.52
f_P	24	0.940 (33)	1.023 (18)	1.94	1.068	14.88	10.53
f_{loss}	12	0.943 (33)	1.000 (1)	1.49	1.997	7.27	10.53
f in (14)	27	0.956 (33)	1.007 (18)	1.57	1.091	14.75	10.52

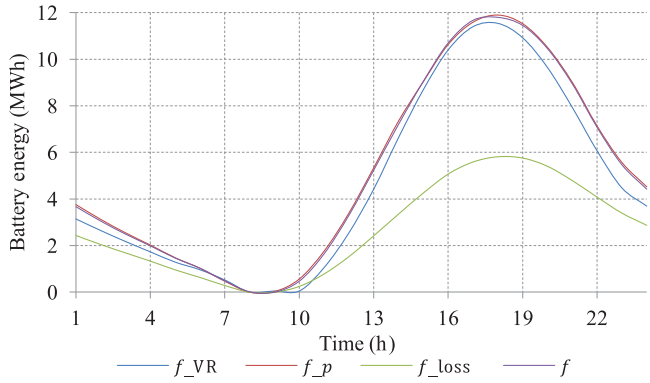

Fig. 8. Battery energy profiles for the various service options.

profiles, net distribution transformer loading, and voltage profiles, respectively.

From Table I, bus 26 is the optimal BESS site for maximum voltage regulation. As shown in Fig. 8, battery discharges from 1:00 A.M. to 8:00 A.M. and then operates at a very slow rate until 10:00 A.M. This improves the morning voltage profile. During peak generation, the BESS drops the voltage at bus 26 to allow reverse power flow to the BESS. Thus, BESS captures peak DG production effectively and delivers it during peak demand to enhance the voltages. The maximum and minimum voltages from f_{VR} optimization are 0.960 and 1.006 p.u., respectively. The peak is reduced to 1.323 MW and energy losses are reduced by 12.22%.

The maximum peak reduction is achieved at bus 24 when controlling peak exclusively (f_P). From Fig. 9, both peak import and export powers are reduced considerably. The peak is reduced by 59.60% compared to the base case. At bus 24, the charge/discharge of the battery not only achieve peak shaving but also assist load leveling as depicted in Fig. 9. During peak PV generation, the battery starts charging and reduces the voltage at bus 24 to allow reverse power flow. During peak demand, the discharge of battery raises the voltage at bus from 6:00 P.M. until midnight while supporting the load. However, no significant improvement in the overall voltage profile is evident and the exclusive peak management has increased the system losses

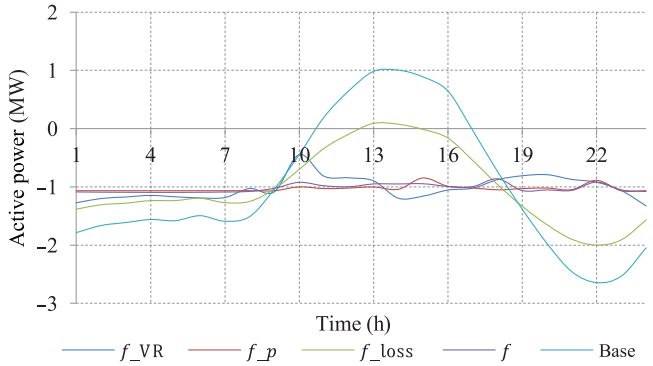

Fig. 9. Distribution transformer loading for various service options.

by 8.06%. From Table I, the optimal size of BESS required to support peak exclusively is greater than for other services.

Bus 12 is the optimal site that achieves most loss reductions when controlling the losses exclusively (f_{loss}). From Table I, the BESS capacity required for the pure control of loss is the lowest. System losses are reduced by 16.92%. However, as illustrated in Figs. 10(c) and 9, the improvement in the lowest voltage and the peak reduction is not as significant.

Bus 27 is the optimal site from the optimization of the cost function (f) for multiple grid services. The BESS effectively captures the reverse power flow and reduces over voltages. The peak export and import powers match very closely with each other and the results from f_P control; thus, it is able to achieve peak shaving as well as load leveling. The maximum and minimum voltages are comparable to that of the f_{VR} optimization and system energy losses are reduced by 12.25%.

The size of the battery required for f minimization is 14.75 MWh. This matches very closely with the BESS sizes for f_{VR} and f_{loss} control. Therefore, based on Table I, the battery is better utilized and maximum tradeoffs are achieved when it is installed for the simultaneous control of multiple services.

The voltage profiles in Fig. 10 illustrate the improvements in the voltages with various controls. From Fig. 10(c), the optimization for exclusive control of system losses does not improve the minimum voltage. However, BESS management for loss control has effectively mitigated the effects of reverse power flow. Furthermore, it is evident from Fig. 10(b) that the BESS installation for exclusive management of peak shows no significant improvement in the lower or upper limit of the voltage profile. Thus, BESS for peak management only does not provide maximum benefits to the grid. Conversely, BESS management for voltage regulation in Fig. 10(a) shows significant improvement in both minimum and maximum voltages. Similar enhanced voltage profile is obtained with the simultaneous control of (14) as shown in Fig. 10(d). This is primarily attributable to the voltage regulation factor in (14).

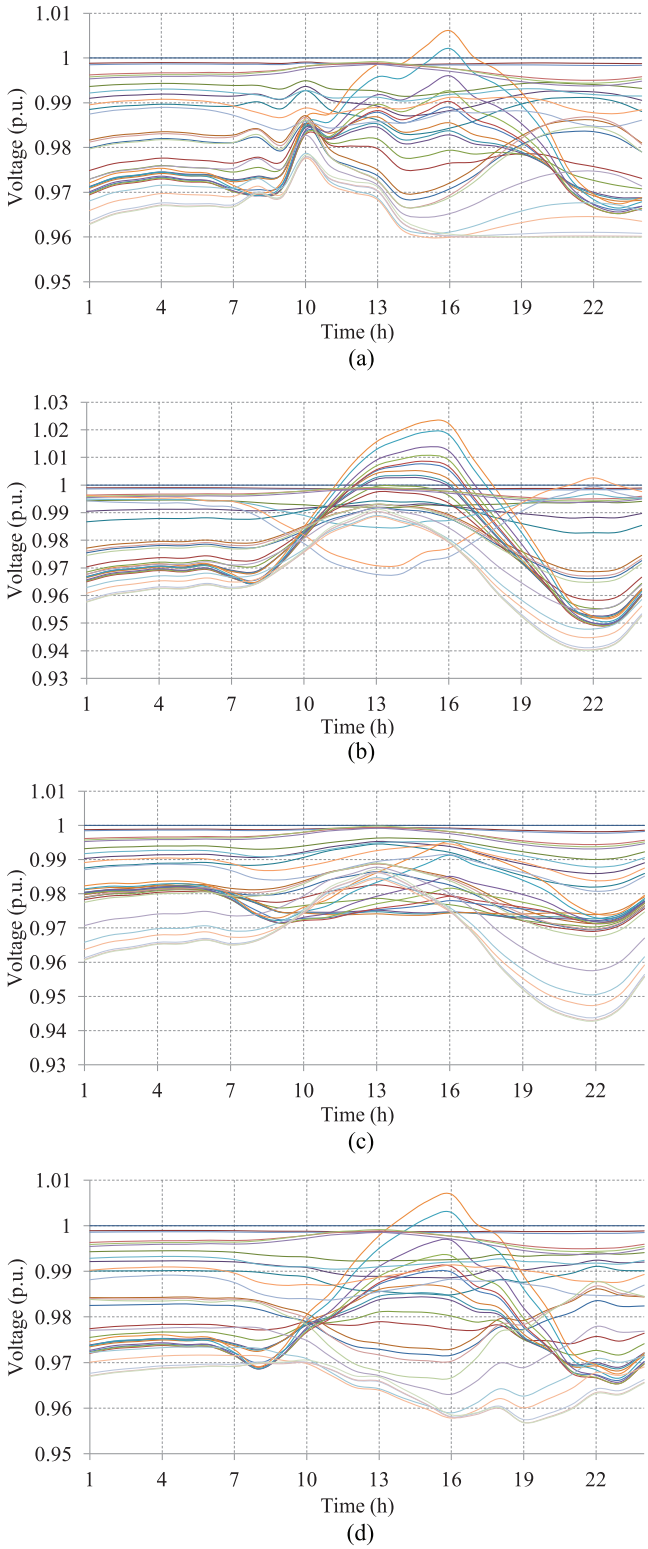

Fig. 10. Voltage profiles for the optimization of (a) f_{VR}, (b) f_p, (c) f_{loss}, and (d) f; legend same as Fig. 7.

B. Test Case 2—LV Distribution System

A similar analysis to that presented for Case 1 is carried out in this section. However, only the buses 10, 15, 17, 21, and 24 are chosen as candidate buses for the study due to geographical constraints and easy accessibility. This LV system represents a typical residential feeder with finely distributed rooftop PVs.

1) Base Operation With No BESS: The net transformer loading and the corresponding voltage profile with no BESS are presented in Figs. 11 and 12, respectively. From Fig. 5, it can be seen that the lateral 1 is independent and separated by the slack bus supplying fewer loads in comparison to the rest

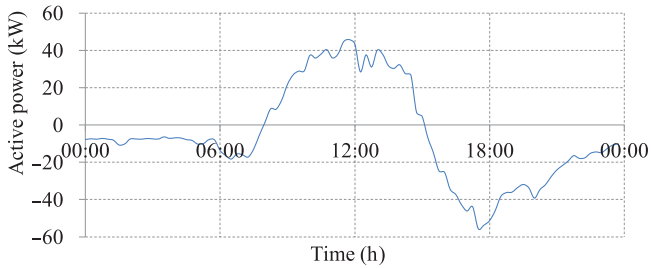

Fig. 11. Distribution transformer loading with no BESS.

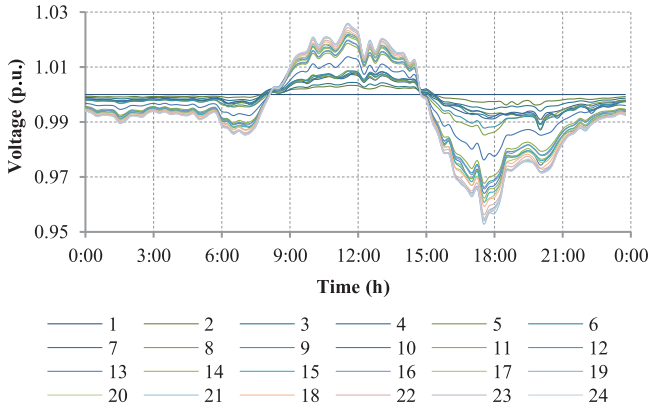

Fig. 12. Voltage profile with no BESS.

TABLE II
SUMMARY OF RESULTS FOR TEST CASE 2

Cost func.	Site (bus no.)	Voltage (p.u.)		E_{loss} kWh	$P_{\max}$ kW	Battery	
		Min (bus#)	Max (bus#)			Size (kWh)	Life (years)
Base		0.953 (21)	1.027 (23)	8.30	55.58		
f_{VR}	17	0.975 (17)	1.011 (17)	7.34	35.08	148.85	15.26
f_P	10	0.960 (10)	1.020 (10)	13.84	28.15	228.88	13.22
f_{loss}	24	0.975 (21)	1.014 (13)	5.27	33.96	93.00	16.10
f in (14)	24	0.975 (24)	1.013 (24)	6.14	31.60	136.26	16.20

of the system. Hence, the voltage deviations and the aggregated load by lateral 1 were not as significant and have no influence on the lateral 2 voltages. Therefore, no battery will be integrated to lateral 1.

2) Simulation Results: Table II summarizes the simulation results of the optimal size, site, BESS life expectancy, voltages, peak power, and losses for different service options. The buses 17, 24, 10, and 24 are identified as the installation sites when optimizing for f_{VR}, f_{loss}, f_p, and f, respectively. Figs. 13–15 show the corresponding battery profiles, distribution transformer loading, and voltage profiles.

From Table II, bus 17 is the optimal BESS site for maximum voltage support. In Fig. 13, the f_{VR} BESS discharges from 12:00 A.M. to 7:45 A.M. As shown in Fig. 15(a), the morning discharge improves the voltage at the bus, consequently

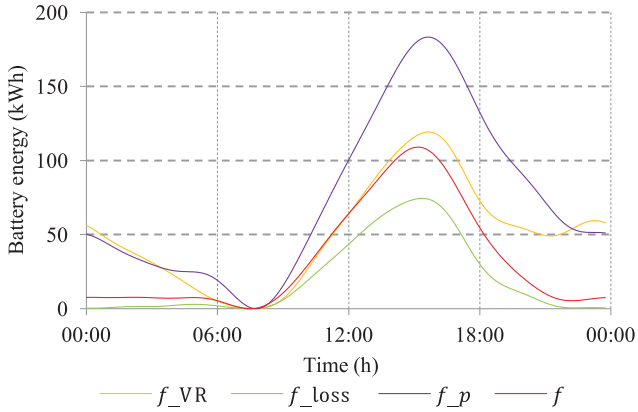

Fig. 13. Battery energy profiles for the various service options.

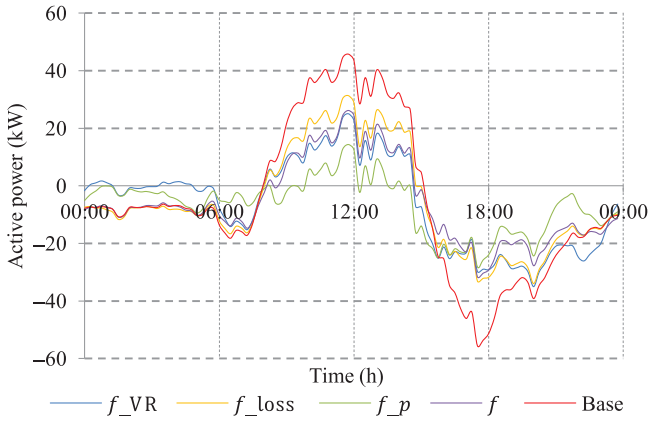

Fig. 14. Distribution transformer loading for various service options.

improving the overall voltage during this period. Now, the power that needs to come from the external grid is nearly zero as shown in Fig. 14. During peak PV generation, the BESS drops the voltage at bus 17 to allow reverse power flow to the BESS. Thus, BESS captures peak DG production effectively and delivers it during peak demand to enhance the voltages. The maximum and minimum voltages from f_{VR} optimization are 0.975 and 1.011 p.u., respectively. The peak is reduced to 35.08 kW and energy losses are reduced by 11.56%.

The optimization shows that the battery at head of feeder enables more peak support while absorbing more PV generation. The maximum peak reduction is achieved at bus 10 when controlling peak exclusively. From Fig. 14, both peak import and export powers are reduced considerably. The peak is reduced by 49.35% compared to the base case. At bus 10, the charge/discharge of the battery not only achieves peak shaving but also assists load leveling as depicted in Fig. 14. During peak PV generation, the battery starts charging and reduces the voltage at bus 10 to allow reverse power flow. Hence, in Fig. 15(b), the minimum voltage of the system is observed at bus 10. During peak demand, the discharge of battery raises the voltage at bus from 3:30 P.M. until midnight while supporting the load. However, no significant improvement in the overall voltage profile is evident and the exclusive peak management has increased the system losses considerably (by 66.74%).

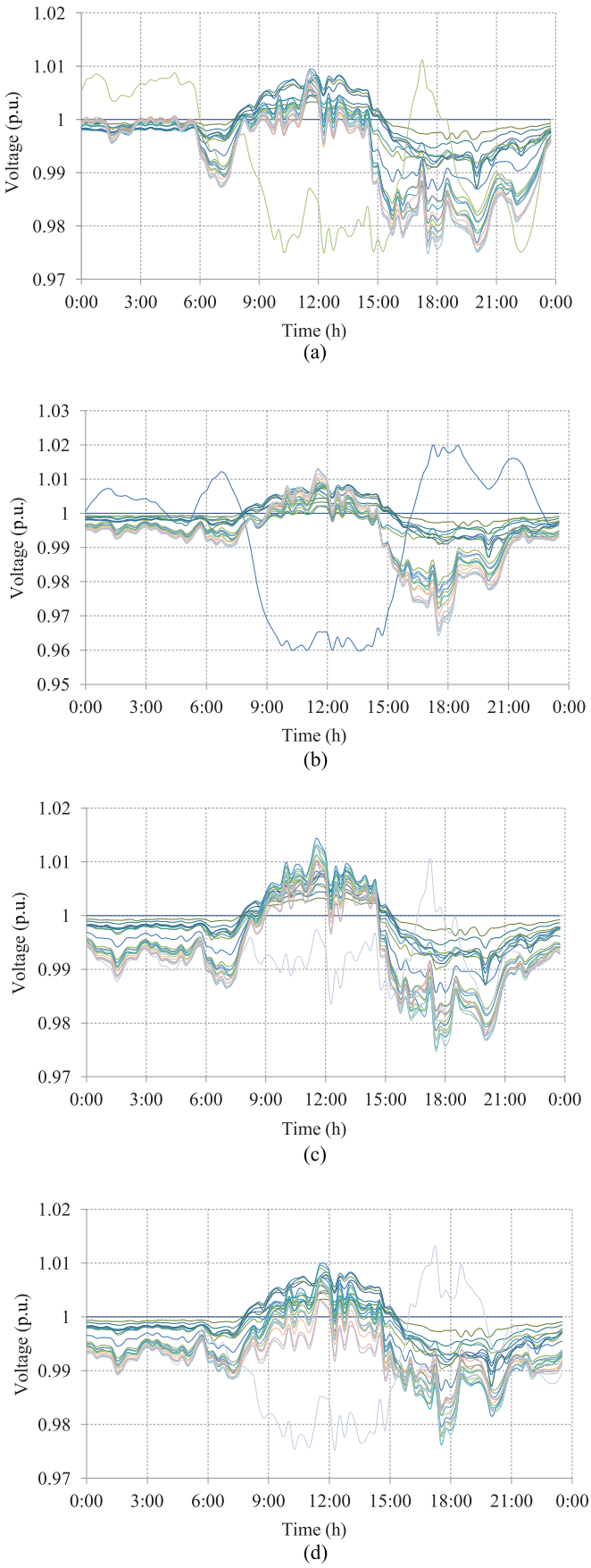

Fig. 15. Voltage profiles for the optimization of (a) f_{VR}, (b) f_p, (c) f_{loss}, and (d) f, respectively; legend same as Fig. 12.

From Table II, the optimal size of BESS required to support peak exclusively is much greater with the lowest life expectancy than for other services.

Bus 24 is the optimal site that achieves most loss reductions when controlling the losses exclusively and is also the optimal site from the optimization of the cost function for multiple grid services. From Table II, the BESS capacity required for the pure control of loss is the lowest. The battery is nearly idle from 12:00 A.M. to 8:00 A.M. However, the battery for multiple grid services discharges from 5:00 A.M. to 7:30 A.M. to support the morning peak. During peak PV generation, battery charges until 3:30 P.M. and discharges from 3:30 P.M. to 10:00 P.M. In this case, the reduction in peak export and import power is almost equal. The power from/to utility is significantly reduced and more evenly distributed over 24 h and managed efficiently. The minimum voltage and maximum voltage observed with battery at bus 24 are 0.975 and 1.013 p.u., respectively.

From the battery energy profiles in Fig. 13, it can be seen that battery energy at the beginning of the day is closer to that at the end of the period. The resultant periodicity and continuity are attributable to the Fourier series approach adopted for battery modeling.

The voltage profiles in Fig. 15 illustrate the improvements in the voltages with various controls. Similar to the Case 1 results, exclusive control of peak using storage does not provide voltage regulation support. Although exclusive control of losses and multiobjective optimization show significant improvement in the overall voltage profile, maximum voltage support is achieved when voltage error (f_{VR}) is controlled exclusively.

VI. Conclusion

This paper proposes a tool that effectively deals with the problem of optimal sizing and dispatch management of BESSs considering various service options. Detailed simulation results show the potential of community-level BESS, controlled by DNO, in addressing distribution system overarching concerns including peak shaving, voltage regulation, and loss reduction for improving system efficiency. Simulations were carried out for an MV and an LV distribution test system. Based on the quantitative analysis, the main conclusions are as follows.

1) The proposed method is able to take the battery daily cycling into consideration, thus optimizes the BESS performance by effectively controlling the cyclic ageing.
2) In most literature, battery systems are installed for peak shaving only. However, based on results in Tables I and II, installation for peak support does not reconcile overvoltage (the primary DG limiting factor) or LV issues. Moreover, it increases system losses considerably.
3) Therefore, the problem needs to be addressed with the aim of improving system voltages to enhance the DG absorption. Maximum tradeoffs are achieved when installing battery considering its ability to simultaneously provide multiple services (Tables I and II).
4) Amount of tradeoffs in terms of voltage regulation, peak shaving, loss reduction, and battery parameters highly depend on the installation site.

5) Base on the results, the benefits and battery parameters are primarily characterized by the system topology as well as the distribution of loads and generation.
6) At any stage, the proposed BESS approach did not violate the capacity limit of distribution system, as the transformer loading is effectively minimized. Therefore, no upgrades will be required for peak support.
7) Adoption and optimal integration of BESS in the next-generation grid will enable better utilization and decentralize management of the available resources improving the ability of the grid to support more demand and host larger quantities of DG.
8) Therefore, the proposed approach will reduce the supply that needs to come from centralized power sources, transmission losses, carbon emission, and related investment costs.

The proposed dispatch management approach is highly suitable for MV or large-scale systems where aggregated load is greatly dominated by the low-frequency diurnal variations, where forecasting errors are low. However, future work will deal with adaptive management of BESS (to improve its ability to respond to changing future predictions) as well as multiple BESS installations and reactive power management to further improve the voltage profile and feeder capacity.

REFERENCES

[1] California Legislative Information. (2010). *Official California Legislative Information Website* [Online]. Available: http://www.leginfo.ca.gov/pub/09-10/bill/asm/ab_2501-2550/ab_2514_bill_20100219_introduced.pdf

[2] D. Green. (2014, Mar.). *Centralized to De-centralized Energy: What Does It Mean for Australia? Draft Discussion Paper* [Online]. Available: https://www.cleanenergycouncil.org.au/policy-advocacy/reports.html

[3] S. McGushin and A. Seeto. (2013, Sep.). *Australia: NSW Electricity Privatisation—The Renewable Assets*, Corrs Chambers Westgarth [Online]. Available: http://www.corrs.com.au/publications/corrs-in-brief/nsw-electricity-privatisation-the-renewable-assets/

[4] R. Charni and M. Maier, "Impact study of collaborative implementation models on total cost of ownership of integrated fiber wireless smart grid communications infrastructures," in *Proc. IEEE Int. Conf. Smart Grid Commun.*, 2013, pp. 31–36.

[5] C. W. Gellings, "Power to the people," *IEEE Power Energy Mag.*, vol. 9, no. 5, pp. 52–63, Sep./Oct. 2011.

[6] C. Lo and N. Ansari, "The progressive smart grid system from both power and communications aspects," *IEEE Commun. Surv. Tuts.*, vol. 4, no. 3, pp. 799–821, Jul. 2012.

[7] X. Lu, W. Wang, and J. Ma, "An empirical study of communication infrastructures towards the smart grid: Design, implementation and evaluation," *IEEE Trans. Smart Grid*, vol. 4, no. 1, pp. 170–183, Mar. 2013.

[8] C. Parrotte. (2014). *Challenges Facing the Electricity Network*, AUPEC [Online]. Available: http://aupec2014.com.au/wp-content/uploads/2014/10/Cameron-_-WE_n12338949_Presentation_-_AUPEC_2014_-_Cameron_Parotte_-_30_September_2014.pdf

[9] International Energy Agency. (2013). *World Energy Outlook: Renewable Energy Outlook*, International Energy Agency, France [Online]. Available: http://www.worldenergyoutlook.org/

[10] D. A. Aviles, F. Guinjoan, J. Barricarte, L. Marroyo, P. Sanchis, and H. Valderrama, "Battery management fuzzy control for grid-tied microgrid with renewable generation," in *Proc. 38th Annu. Conf. IEEE Ind. Electron. Soc. (IECON)*, 2012, pp. 5607–5612.

[11] C. A. Silva-Monroy and J. Watson, "Integrating energy storage devices into market management systems," *Proc. IEEE*, vol. 102, no. 7, pp. 1084–1093, Jul. 2014.

[12] A. Cody, M. C. Such, D. Chen, J. Gonzalez, and M. Grady, "Battery energy storage for enabling integration of distributed solar power generation," *IEEE Trans. Smart Grid*, vol. 3, no. 2, pp. 850–857, Jun. 2012.

[13] Z. Wang, C. Gu, F. Li, P. Bale, and H. Sun, "Active demand response using shared energy storage for household energy management," *IEEE Trans. Smart Grid*, vol. 4, no. 1, pp. 1888–1897, Dec. 2013.

[14] Y. Riffonneau, S. Bacha, F. Barruel, and S. Ploix, "Optimal power flow management for grid connected PV systems with batteries," *IEEE Trans. Sustain. Energy*, vol. 2, no. 3, pp. 309–320, Jul. 2011.

[15] S. Teleke, M. E. Baran, S. Bhattacharya, and A. Q. Huang, "Rule-based control of battery energy storage for dispatching intermittent renewable sources," *IEEE Trans. Sustain. Energy*, vol. 1, no. 3, pp. 117–124, Oct. 2010.

[16] M. J. E. Alam, K. M. Muttaqi, and D. Sutanto, "Mitigation of rooftop solar PV impacts and evening peak support by managing available capacity of distributed energy storage systems," *IEEE Trans. Power Syst.*, vol. 28, no. 4, pp. 3874–3884, Nov. 2013.

[17] W. D. Grossmann, I. Grossmann, and K. W. Steininger, "Distributed solar electricity generation across large geographic areas, Part I: A method to optimize site selection, generation and storage," *Renew. Sustain. Energy Rev.*, vol. 25, pp. 831–843. Sep. 2013.

[18] D. Q. Hung and N. Mithulananthan, "Community energy storage and capacitor allocation in distribution systems," in *Proc. Australas. Univ. Power Eng. Conf. (AUPEC)*, 2011, pp. 1–6.

[19] S. X. Chen, H. B. Gooi, and M. Q. Wang, "Sizing of energy storage for microgrids," *IEEE Trans. Smart Grid*, vol. 3, no. 1, pp. 142–151, Mar. 2012.

[20] G. Parkinson. (2013, Dec.). *EOS: Utility Scale Battery Storage Competitive With Gas* [Online]. Available: http://reneweconomy.com.au/2013/eos-utility-scale-battery-storage-competitive-with-gas-36444

[21] G. Parkinson. (2014, Aug.). *How Far Away is Grid Parity for Residential Battery Storage?*, Renewable Economy [Online]. Available: http://reneweconomy.com.au/2014/how-far-away-is-grid-parity-for-residential-battery-storage-62637

[22] A123 Energy Solutions. (2013). *A123 Systems ALM 12V& User's Guide, A123 Energy Solutions* [Online]. Available: http://www.a123energy.com

[23] P. Rong and M. Pedram, "An analytical model for predicting the remaining battery capacity of lithium-ion batteries," *IEEE Trans. Very Large Scale Integr. Syst.*, vol. 14, no. 5, pp. 441–451, May 2006.

[24] A. Millner, "Modeling lithium-ion battery degradation in electric vehicles," in *Proc. IEEE Conf. Innov. Technol. Effic. Reliable Elect. Supply (CITRES)*, 2010, pp. 349–356.

[25] H. Rahimi-Eichi, U. Ojha, F. Baronti, and M. Chow, "Battery management system: An overview of its application in the smart grid and electric vehicles," *IEEE Ind. Electron. Mag.*, vol. 7, no. 2, pp. 4–16, Jun. 2013.

[26] N. Jayasekara, P. Wolfs, and S. Subawickrama, "A Fourier series based approach to the periodic optimization of finely dispersed battery storage," in *Proc. Australas. Univ. Power Eng. Conf. (AUPEC)*, Sep. 2011, pp. 1–6.

[27] A. Alfaris. (2010). *Multidisciplinary System Design Optimization: Multiobjective Optimization*, Massachusetts Institute of Technology [Online]. Available: http://ocw.mit.edu/courses/engineering-systems-division/esd-77-multidisciplinary-system-design-optimization-spring-2010/lecture-notes/MITESD_77S10_lec14.pdf

[28] AEMC, "Possible future retail electricity price movements: 1 July 2012 to 30 June 2015," Sydney, Australia, Electricity Price Trends Rep., Mar. 2013.

[29] Live Performance Australia. (2014). *Design Guide: Managing Peak Demand in Live Performance Venues* [Online]. Available: http://liveperformance.com.au/sites/liveperformance.com.au/files/resources/design_guide_-_managing_peak_energy_demand_in_venues.pdf

[30] A. Domahidi, A. U. Zgraggen, M. N. Zeilinger, M. Morari, and C. N. Jones, "Efficient interior point methods for multistage problems arising in receding horizon control", in *Proc. IEEE 51st Annu. Conf. Decis. Control (CDC)*, Maui, HI, USA, Dec. 2012, pp. 668–674.

[31] V. M. da Costa, N. Martins, and J. L. R. Pereira, "Developments in the Newton Raphson power flow formulation based on current injections," *IEEE Trans. Power Syst.*, vol. 14, no. 4, pp. 1320–1326, Nov. 1999.

[32] P. A. N. Garcia, J. L. R. Pereira, S. Carneiro, V. M. da Costa, and N. Martins, "Three-phase power flow calculations using the current injection method," *IEEE Trans. Power Syst.*, vol. 15, no. 2, pp. 508–514, May 2000.

[33] B. Venkatesh, R. Ranjan, and H. B. Gooi, "Optimal reconfiguration of radial distribution systems to maximize loadability," *IEEE Trans. Power Syst.*, vol. 19, no. 1, pp. 260–266, Feb. 2004.

[34] Y. M. Atwa, E. F. El-Saadany, M. M. A. Salama, R. Seethapathy, M. Assam, and S. Conti, "Adequacy evaluation of distribution system including wind/solar DG during different modes of operation," *IEEE Trans. Power Syst.*, vol. 26, no. 4, pp. 1945–1952, Nov. 2011.

[35] D. Q. Hung and N. Mithulananthan, "Alternative analytical approaches for renewable DG allocation for energy loss minimization," in *Proc. IEEE Power Energy Soc. Gen. Meeting*, 2012, pp. 1–10.

Nadeeshani Jayasekara (S'06) received the B.Eng. degree from Curtin University, Perth, W.A., Australia, in 2009. She is currently pursuing the Ph.D. degree in electrical power engineering at Curtin University, upon receiving Australian Postgraduate Awards (APA) scholarship.

Her research interests include distributed generation, distributed energy storage, impacts of DG and storage, power quality, power system capacity optimization, and power dispatch management.

Mohammad A. S. Masoum (S'88–M'91–SM'05) received the B.S., M.S., and Ph.D. degrees in electrical and computer engineering from the University of Colorado, Boulder, CO, USA, in 1983, 1985, and 1991, respectively.

Currently, he is a Professor with the Electrical and Computer Engineering Department, Curtin University, W.A., Australia. He is the coauthor of *Power Quality in Power Systems and* Electrical *Machines* (Elsevier, 2008) and *Power Conversion of Renewable Energy Systems* (Springer, 2011). His research interests include optimization, power quality, and stability of power systems and electric machines, as well as distributed generation.

Peter J. Wolfs (M'79–SM'97) is the Director of the Power and Energy Centre, Central Queensland University, Rockhampton, Qld., Australia. He has authored more than 200 technical journal and conference publications in electrical engineering. His research interests include smart grid technology especially in regard to distributed renewable resources and energy storage impacts on system capacity and power quality, the impact of electric vehicles, the support of weak rural feeders, and remote area power supply.

Prof. Wolfs is the Chair of the Australasian Committee for Power Engineering (ACPE), a Fellow of Engineers Australia, and a Registered Professional Engineer in the State of Queensland.